

Design and operation of an *in situ* microchannel alignment-detection system

Brian Robertson, David Kabal, Guillaume C. Boisset, Yongsheng Liu, William M. Robertson, Mohammad R. Taghizadeh, and David V. Plant

The design of an alignment-detection system that uses off-axis diffractive elements and photodetectors is presented. The system was developed to detect the real-time misalignment of an array of optical beams as they pass through a microchannel relay. The design of this scheme is presented along with experimental results obtained from a prototype detection system. © 1998 Optical Society of America
OCIS codes: 220.1140, 050.1970, 200.4650.

1. Introduction

The past few years have seen an increasing interest in the field of free-space interconnection technology. Research in this area has been motivated primarily by the problems that conventional electrical interconnection technology faces in meeting the projected throughputs required by future computing and switching systems.

Microchannel free-space interconnects have a number of advantages over conventional lens systems, including compactness, scalability, a low latency, and a low component count. In addition, they do not suffer from the field-dependent aberrations that affect conventional lens relays. However, to implement an interconnect based on microchannel relays, it is necessary to meet tight alignment tolerances between the lenslet arrays themselves and between the lenslet arrays and the optical signal beams. The alignment of lenslet arrays with respect to each other can be achieved by use of a variety of methods, including fiducial alignment marks,¹ moiré patterns,² and interferometric alignment elements.³ In this paper a novel, to our knowledge, technique for aligning an array of signal beams with respect to a

lenslet array is presented. The system uses a combination of off-axis lenslets, high-frequency gratings, and photodetectors to generate real-time alignment information. These data can be used to optimize the transverse alignment of the signal beams with respect to the lenslet array and to monitor the positional stability of the interconnect. The design of the alignment-detection system (ADS) is presented, along with the experimental performance of a prototype scheme.

2. Operation of the Alignment-Detection System

A schematic outline of an ADS designed to detect the alignment of an array of beams generated by a Fourier plane fan-out grating with respect to a microchannel relay system is shown in Fig. 1. In addition to the $N \times N$ array of signal beams, the grating is optimized to produce four extra alignment beams, as shown in Fig. 1. These alignment beams are used by the ADS to detect the relative position of the array of signal beams with respect to the microchannel relay. A more detailed layout of the ADS is shown in Figs. 2 and 3. The alignment beams are incident on binary-phase off-axis lenslets (OA1–OA4) fabricated on the first lenslet array (LA₁). These components collimate a portion of the light and diffract it at an angle to the incident beam. The collimated beams propagate away from the central set of lenslets and bounce off mirrors (M1–M4) positioned on the rear side of the lenslet substrate onto a set of high-frequency gratings (HFG1–HFG4) (fabricated on the same side of the substrate as the lenslets) that are arranged to act as apertures. Single-element detectors on a donut-shaped printed circuit board (PCB) collect the transmitted light of the resulting $m = +1$ diffraction order. The inner diameter of the donut

B. Robertson, D. Kabal, G. C. Boisset, Y. Liu, and D. V. Plant are with the Department of Electrical Engineering, McGill University, Montréal, Québec H3A 2A7, Canada. W. M. Robertson is with the Department of Physics and Astronomy, Middle Tennessee State University, Box X-116, Murfreesboro, Tennessee 37132. M. R. Taghizadeh is with the Department of Physics, Heriot-Watt University, Riccarton, Edinburgh EH14 4AS, Scotland.

Received 17 September 1997; revised manuscript received 8 April 1998.

0003-6935/98/235368-09\$15.00/0
© 1998 Optical Society of America

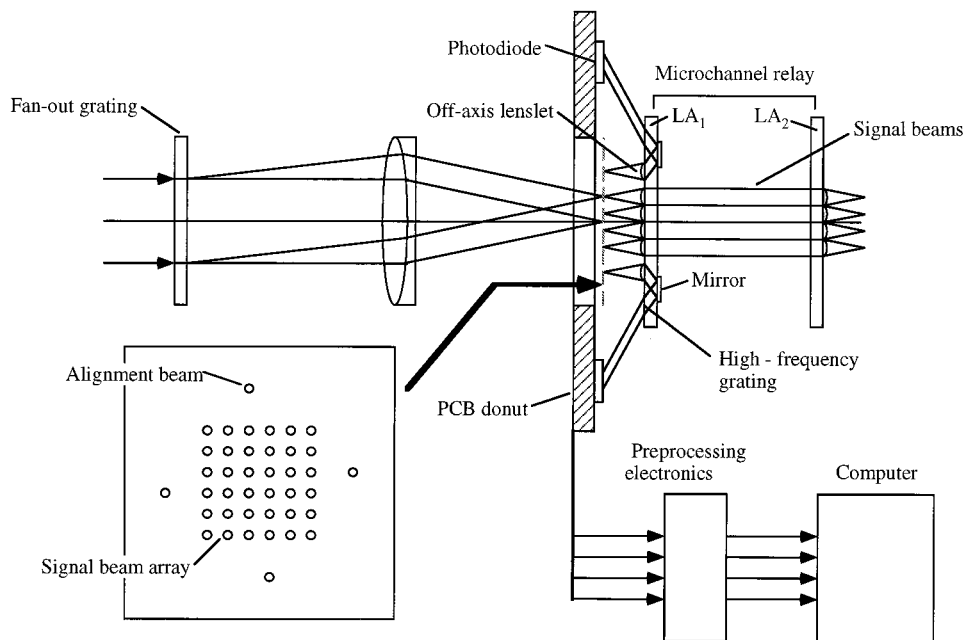


Fig. 1. Schematic overview of the ADS.

must be calculated carefully to ensure that none of the incident light is blocked by the donut PCB. Finally, the optical signals are converted into voltage signals from which the relative misalignment may be determined.

From Fig. 2 it can be seen that the high-frequency gratings are placed so as to pass alternating sides of the alignment beams when the system is perfectly positioned. Thus when the interconnect is correctly aligned each detector will pick up the same amount of light. As the incident beams are misaligned, error signals similar to those produced by a quadrant de-

tector (a four-element photodiode used to detect the position of an optical beam) will be observed. For example, if the beams are misaligned in the $+x$ direction, more light will be diffracted by HFG3 than by HFG1 onto the corresponding photodiodes. It should be noted, however, that the beams will be clipped by OA3 and OA1, which will reduce the amount of light reaching HFG3 and HFG1. The resulting difference in voltage signals can be used to determine the actual misalignment.

The ADS could operate just as effectively if the high-frequency gratings were replaced by metal apertures that blocked alternating sides of the alignment beams. However, using a diffractive element is advantageous, as it increases the propagation angles of the beams with respect to the substrate and allows the photodiodes to be placed farther away from the center of the signal-beam array. This, in turn, increases the inner diameter of the PCB donut, thereby reducing clipping effects. In addition, as the high-frequency gratings are fabricated at the same time as the lenslets, the positional accuracy of these elements will be determined primarily by the precision of the original amplitude mask. Using metal apertures introduces an extra fabrication step that could increase the relative alignment error.

It is assumed that the binary-phase off-axis diffractive lenslets are required to take a normally incident spherically diverging wave front, collimate it, and redirect it at an angle ψ with respect to the incident beam within the substrate, as shown in Fig. 3. The theory governing off-axis lenslets and their application as optical interconnects have been discussed previously.^{4,5} The spatially varying local grating period $T(x, y)$ can be calculated from the grating equation

$$(\sin \alpha_m - \sin \alpha_i) = m\lambda/T(x, y), \quad (1)$$

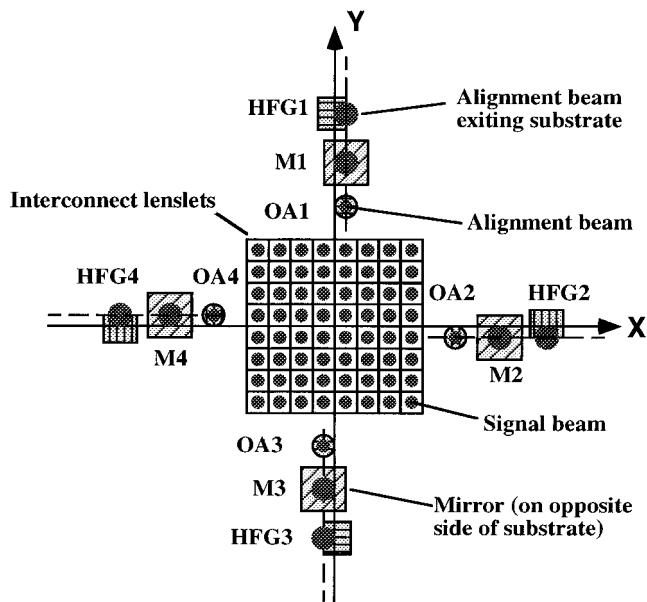


Fig. 2. Top view of the ADS with the signal beams perfectly aligned.

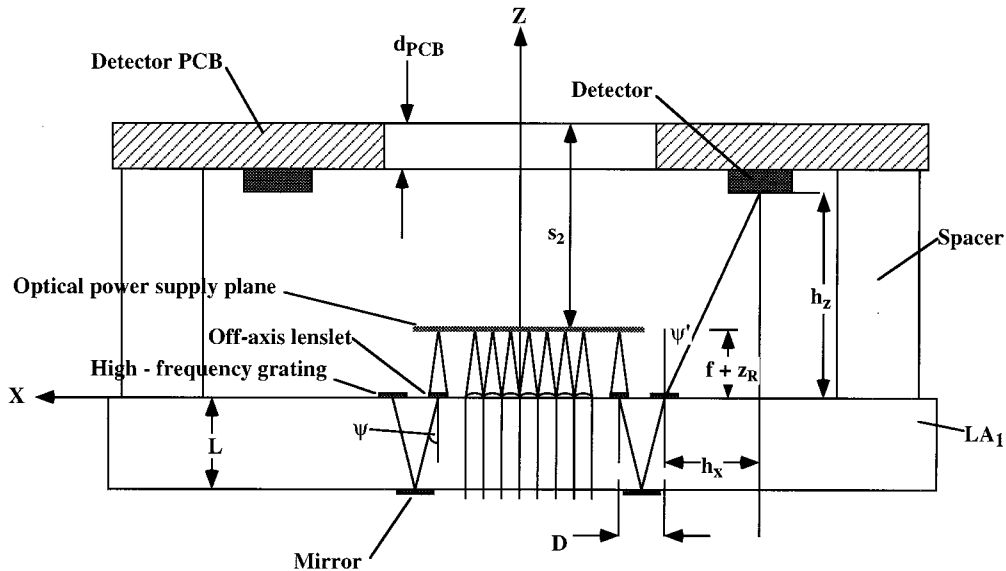


Fig. 3. Side view of the ADS.

where λ is the operating wavelength, n is the refractive index of the substrate, α_i is the incident angle, and α_m is the angle of the m th diffracted beam. In particular, our analysis concentrates on the +1 diffraction order, which must meet the condition $\alpha_{+1} = \psi$. Thus to collimate the incident ADS beams it is necessary that the off-axis lenslets have a focal length equal to z_1 , the distance from the incident spot array to the lenslet array.

If the width of the substrate is L , the distance from the center of the off-axis lenslet to the center of the high-frequency grating, D , is given by

$$D = 2L \tan \psi, \quad (2)$$

and the distance from the center of the high-frequency grating to the center of the photodiode, h_x , is given by

$$h_x = h_z \tan[\arcsin(\lambda/\Lambda + n \sin \psi)], \quad (3)$$

where h_z is the height from the lenslet substrate to the photodiode and Λ is the period of the high-frequency grating. The undiffracted zeroth order will be incident on the same plane at a distance

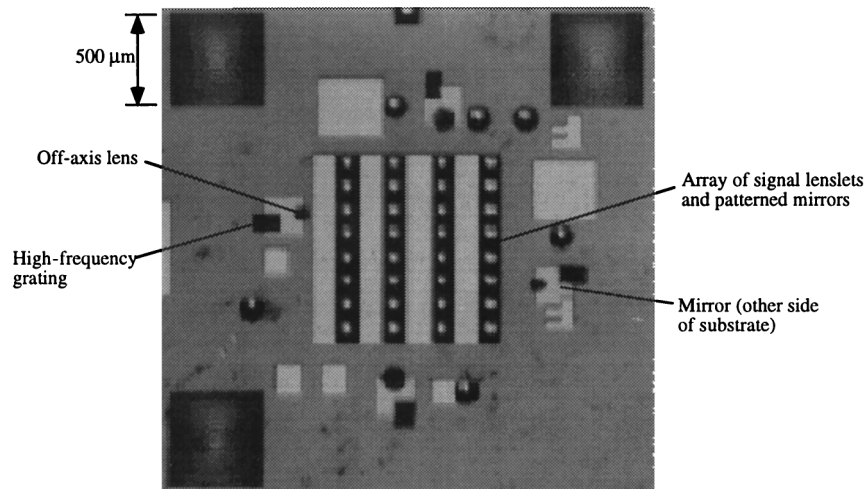
$$h_0 = h_z \tan[\arcsin(n \sin \psi)]. \quad (4)$$

The difference between these two terms, $h_x - h_0$, sets the maximum dimensions of the photodiode.

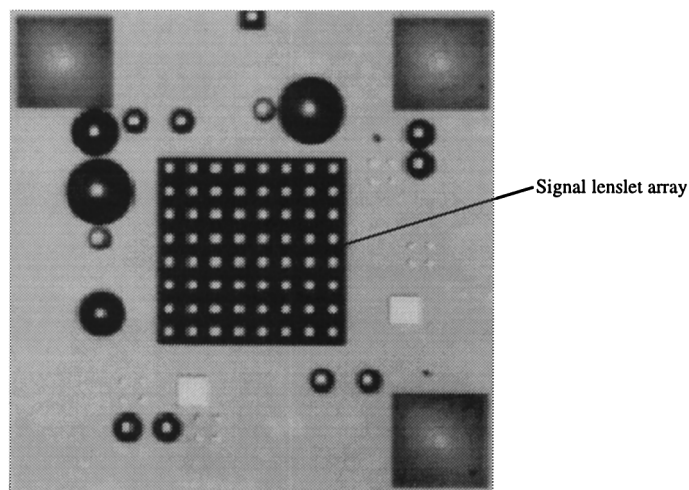
3. Experimental Test System

To verify the practicality of this technique, we incorporated an ADS within a microchannel relay. This microchannel interconnect formed part of a hybrid relay system that was designed for use within a prototypical free-space photonic backplane.⁶ Optical backplanes that merge complementary metal-oxide semiconductor (CMOS) processing with free-space optical interconnects between PCB's were proposed in Ref. 7. These systems differ from prior optical

backplanes in that they support intelligence directly in the optoelectronic interconnect. The intelligence coupled with the potential for data rates of over 155 Mbits per optical communication channel yields capabilities that were not possible with prior optical systems. The architectural design and capabilities of intelligent optical backplanes can be found in Refs. 7 and 8. Figure 4 illustrates the hybrid-interconnection scheme developed for this prototype system. For separating the various signal and power-supply beams, both polarization components and patterned-mirror arrays are used. At each stage light from an external-cavity stabilized laser diode operating at 850 nm enters the circuit by means of a single-mode polarization-maintaining fiber. The light is collimated and passes through a quarter-wave plate to produce circularly polarized light. A nonseparable multiple-phase fan-out grating and Fourier transform lens are then used to generate the requisite array of beams in front of LA₁. Risley beam steerers and an adjustable tilt plate are used to align the power-supply beams accurately with respect to the interconnection assembly. The light is then relayed by means of LA₁ and LA₂ to the modulators on the first CMOS-SEED (self-electro-optic device) device array (DA₁). The modulated signal beams travel back through LA₂, are reflected by the polarizing beam splitter (PBS), and relayed by means of the telecentric relay system to LA₃, where they are reflected by pixelated mirrors onto the second CMOS-SEED device array (DA₂). Note that the pixelated mirrors are fabricated as part of the lenslet array, thereby reducing the overall complexity of the system. The mirrors consist of a silver reflective layer with a gold cap layer and are operated in an internal reflection mode. The signal beams are then finally focused by LA₄ onto the corresponding receivers on the second CMOS-SEED device array (DA₂). The interconnect was designed to operate with a 4 ×



(a)



(b)

Fig. 5. Photographs of (a) the OPSLA showing the ADS and (b) the CMOS-SEED lenslet array.

beam that propagates at an angle of 10° within the substrate. For obtaining z misalignment information, two different-diameter off-axis lenslets are used: OAL1 and OAL3 have a diameter of g_1 and OAL2 and OAL4 have a diameter of g_2 . By monitoring of the ratio of the signals received, it was possible to determine the longitudinal misalignment Δz . The theoretical $1/e^2$ Gaussian beam radius w_L of a perfectly aligned, unaberrated beam at the front side of the OPSLA is given by

$$w_L = w_0 \{1 + [z_1 \lambda / (\pi w_0^2)]^2\}^{1/2}.$$

Thus, as $w_0 = 6.47 \mu\text{m}$, it follows that $w_L = 39.1 \mu\text{m}$. Setting $g_1 = 123 \mu\text{m}$ and $g_2 = 78.25 \mu\text{m}$ will result in an ideal ratio of signals of 1 to 0.86 when all translational misalignments are corrected for. The theoretical variation in the ratio of the alignment voltages as a function of longitudinal misalignment Δz can be

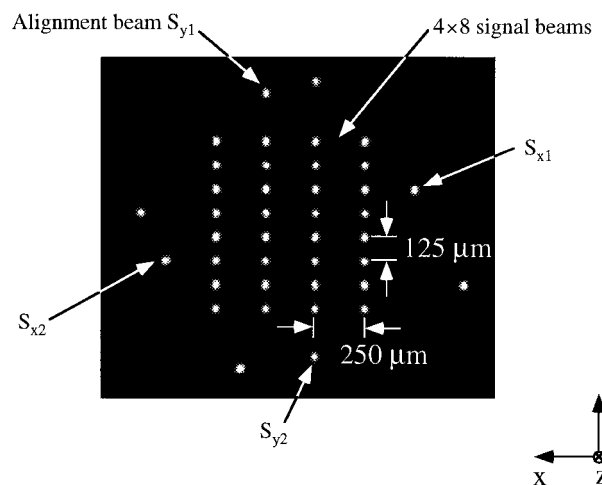


Fig. 6. Photograph of the spot array generated by the optical power supply.

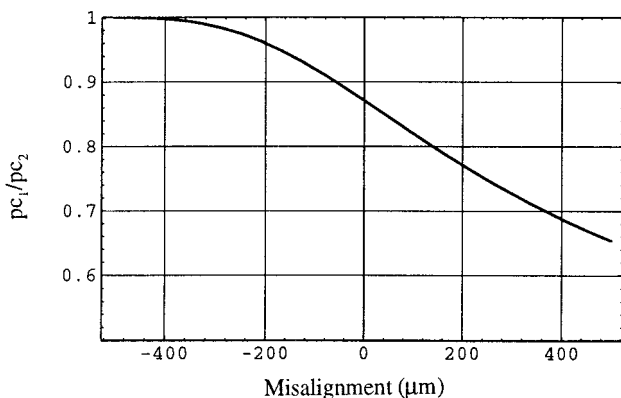


Fig. 7. Theoretical variation of pc_1/pc_2 with the longitudinal misalignment Δz .

determined by the calculation of the ratio of the integrals pc_1/pc_2 , where

$$pc_1 = \int_0^{g_1/2} 2\pi r I(r) dr,$$

$$pc_2 = \int_0^{g_2/2} 2\pi r I(r) dr,$$

and $I(r) = I(z_1 + \Delta z) \exp[-2r^2/w(z_1 + \Delta z)^2]$. Figure 7 shows the theoretical dependence of pc_1/pc_2 on the longitudinal misalignment. The internal diffraction angle was chosen to be 10° to meet the fabrication restrictions associated with the diffractive optical element manufacturing process.

C. Mirrors

A set of four miniature mirrors was fabricated on the opposite side of the OPSLA. These elements consisted of a silver reflective layer with a gold cap layer and were operated in an internal reflection mode. The dimensions of the mirrors were $200 \mu\text{m} \times 200 \mu\text{m}$.

D. High-Frequency Gratings

High-frequency binary-phase gratings were fabricated on alternating sides of the optical beam axes, as shown in Fig. 2. The period of these elements was $3 \mu\text{m}$, and the beams were diffracted at an angle of 32.4° with respect to the surface of the grating. These components had dimensions of $100 \mu\text{m} \times 150 \mu\text{m}$. As the thickness of the substrate was $500 \pm 30 \mu\text{m}$, the distance from the center of the off-axis lenslet to the center of the corresponding high-frequency grating was $176.3 \mu\text{m}$ [Eq. (2)].

E. Printed Circuit Board Donut

The four photodiodes were directly mounted on the PCB, as shown in Fig. 8. The donut-shaped PCB is a single-layer, 0.062-in.-thick (0.157-cm-thick) FR-4 (Fire Retardant Grade 4) board, with a cover layer to prevent shorting of solder joints. The board is immersion plated with gold to make it wire bondable.

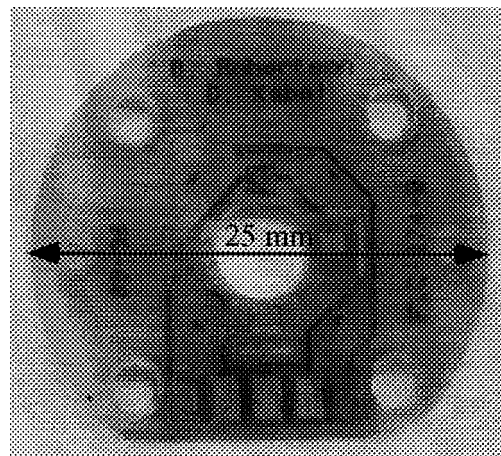


Fig. 8. PCB donut.

Four pads make the back contact with the p-n photodetectors, and the top contact is wire bonded with an aluminum-wedge ultrasonic wire bonder onto adjacent pads. Under a microscope, the p-n photodetectors are glued onto the back contact pad by use of silver-filled epoxy. The back contact pad is a 1.5-mm square pad. The p-n photodetectors are 1.0-mm squares. A standard, five-conductor flat ribbon-cable assembly is soldered onto the edge of the board to connect the board to biasing and readout circuitry.

F. Preprocessing Electronics

In this subsection the design for the ADS preprocessing electronics is described. Four optical alignment signals, S_{x1} , S_{x2} , S_{y1} , and S_{y2} , are incident on the off-axis lenslets (OA1–OA4) and are diffracted onto the four photodetectors (D_{x1} , D_{x2} , D_{y1} , D_{y2}). When the system is perfectly aligned identical photocurrents are generated by D_{x1} and D_{x2} and by D_{y1} and D_{y2} . If the optical power-supply beams are misaligned with respect to the OPSLA by a distance (Δx , Δy) or are rotated by an angle of θ_z about the z axis, the photocurrents will be different. These trends allow us to detect and ultimately correct the misalignment error. In addition, as the two sets of off-axis lenslets have different diameters, the ratio of the photocurrents allows us to detect Δz misalignment.

For estimating the throughput of the current ADS design (Fig. 3), the following losses were assumed: a Fresnel reflection loss at the off-axis lenslet of 4%, an efficiency for the off-axis lenslet of 40% (binary element), 98% reflection from the silver mirror, and an efficiency for the high-frequency grating of 40% (binary element). This results in an overall throughput of 15%. The optical power budget for the interconnection system allows for a power in each beam generated by the optical power supply of approximately $690 \mu\text{W}$. Thus the maximum amount of light P_{max} that can reach the alignment detectors is $103.5 \mu\text{W}$. However, if the optical power-supply beams are aligned properly with respect to the lenslet array, only half of this light will reach each photode-

Table 1. Photodiode Parameters

Parameter	Value
Die outside dimensions	1 mm × 1 mm
Active area	0.93 mm × 0.93 mm = 0.86 mm ²
Die thickness	270 μm
Dark current	50 nA @ V _r = 10 V
Spectral response peak	850 nm
Response time (minimum)	2 μs @ 0 V
V _{reverse} (maximum)	30 V
Saturation intensity	100 μW/mm ²

tector. As a result, the alignment detectors ideally should receive $P_{inc} = 51.75 \mu\text{W}$. Depending on the relative misalignment, this value can approach 0 mW or can increase to a maximum of approximately 103.5 μW. The photodetectors must therefore exhibit a linear response for incident powers ranging between $P_{inc} = 0 \mu\text{W}$ and $P_{inc} = 103.5 \mu\text{W}$. The parameters of the photodetectors that were used in this system are given in Table 1.

The electronic circuit used with the system is shown in Fig. 9. The photodiodes are operated in a photoconductive mode so that each photocurrent i_p produces a voltage across a load resistor (R_{x1} , R_{x2} , R_{y1} , and R_{y2}) that is linearly proportional to the incident optical power. For simplicity it is assumed that the load resistances are all equal to R_L . The corresponding signal voltages (V_{x1} , V_{x2} , V_{y1} , and V_{y2}) are then sent to the analog-digital board by means of unity-gain buffers. From these signal voltages the following alignment parameters can be calculated:

- (1) A Δx misalignment of $\alpha(V_{x2} - V_{x1})$.
- (2) A Δy misalignment of $\beta(V_{y2} - V_{y1})$.
- (3) A Δz misalignment of $\gamma[(V_{x1} + V_{x2})/(V_{y1} + V_{y2})]$.

Here α , β , and γ are functions of the measured voltages. When all these terms equal zero or, in the case of a z misalignment, the correct signal ratio of 0.86, the signal beams will be perfectly aligned with respect to the OPSLA (balanced signals from each detector). In addition, there will be zero rotational misalignment.

5. Experimental Results

Figure 10 shows the final packaged ADS-microchannel relay assembly. To test the performance of this system, we mounted the optical power supply on a computer-controlled stepper-motor stage, and the corresponding signal voltages were measured as the stepper motor translated the optical beams across the OPSLA. The variation in the alignment voltages V_{x1} and V_{x2} as functions of the stepper motor position are shown plotted in Fig. 11. From this result it can be seen that the ADS behaves as expected; at the optimum alignment position the two voltages are approximately equal, and as the system becomes misaligned one voltage increases and the other decreases as the beams are translated across

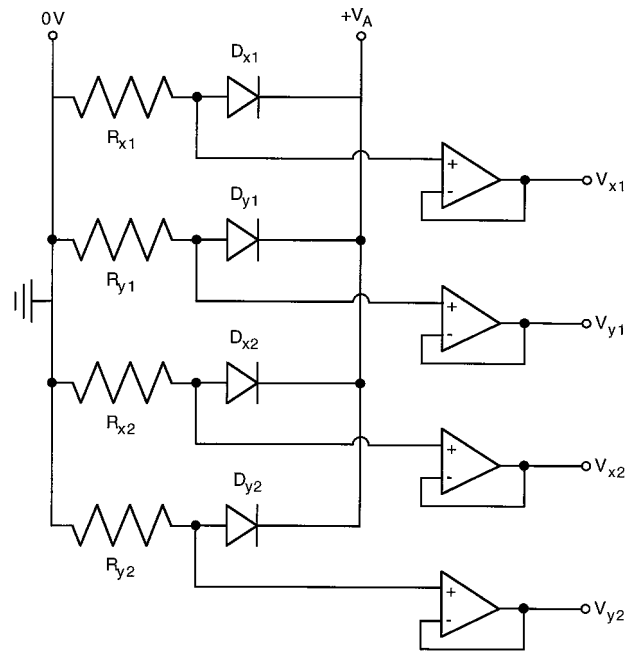


Fig. 9. Electronic preprocessing circuitry.

the lenslet array. In addition, the ADS is extremely sensitive to transverse misalignment, as a measurable voltage difference occurs after only a few micrometers of travel. There is, however, a difference between the maximum signal voltages obtained. For V_{x1} the signal peaks at 9.5 V, and for V_{x2} the signal peaks at 7.5 V. To compensate for this discrepancy, we introduce a scaling factor of $\kappa = (V_{x1}/V_{x2}) = 1.263$, derived from the peak alignment voltages. Using this value to scale the V_{x2} curve results in a null voltage occurring at $\Delta x = -7 \mu\text{m}$. This is the position at which the array of optical signal beams are correctly aligned with respect to the OPSLA.

This difference in voltage can in part be attributed to nonuniformity of the ADS beams (measured non-uniformity of $\pm 4\%$), unequal resistor values (uniformity measured to be $\pm 2\%$), and variations in the responsivity of the photodiodes. The positioning of the photodiodes is not critical as long as they are bigger than the size of the optical alignment beams. Other possible causes for this discrepancy in maximum signal voltage include nonuniformities in the micro-optics used to implement the ADS and possible dust contamination. For proper operation the ADS should be calibrated to take into account these errors.

Noise arises from two sources: fluctuations in the incident laser beam and noise in the photodiode and detector circuitry. As the alignment beams are all derived from the same laser source, the noise contribution will be identical for all four alignment beams. However, as the transverse-misalignment information is determined by the difference in the received power, laser noise will affect the resulting alignment signal. Thus a low-noise laser system will be required by this ADS. Noise in the photodiode and

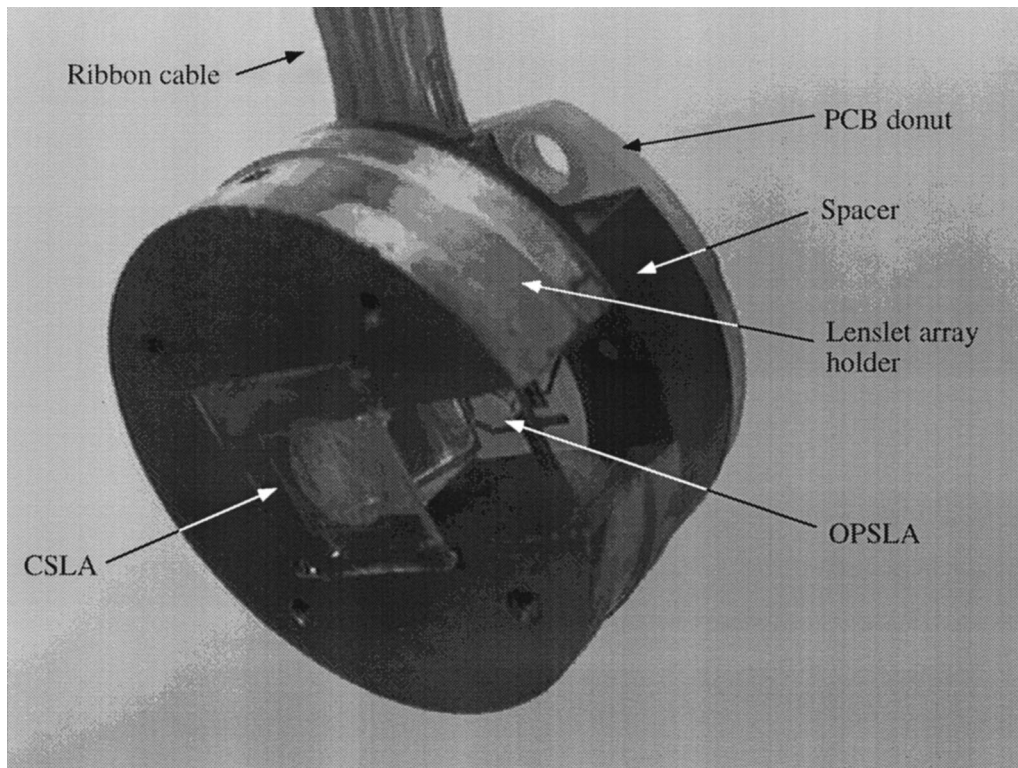


Fig. 10. Photograph of the ADS-microchannel relay assembly. The outer diameter of the assembly is 25 mm.

receiver circuitry will also affect the final alignment signal voltages.

6. Conclusions

An ADS designed to detect the position of an array of signal beams with respect to a microchannel relay has been described. The system uses a combination of off-axis diffractive lenslets, high-frequency grating apertures, and photodiodes to produce real-time alignment signals similar to those produced by a quadrant detector. Experimental results obtained from a prototype system verify the system's performance, with measurable voltage differences being measured after only a few micrometers

of misalignment. However, there is an imbalance between the signal voltages owing in part to the nonuniformity of the ADS signal beams and preprocessing electronics. To improve the accuracy of the setup one should calibrate the ADS to take these errors into account.

Future research is planned to concentrate on improving the uniformity of the response and on integrating the photodiodes with the optical components to produce smart lenslet arrays. Such arrays are capable of sensing the relative alignment of an array of beams passing through them.

D. V. Plant acknowledges support from the Canadian Institute of Telecommunications Research. In addition, this study was also supported by the Nortel/National Science and Engineering Research Council (NSERC) Chair in Photonics Systems. The multiple-level phase gratings were obtained from the Defense Advanced Research Projects Agency-sponsored Consortium for Optical and Optoelectronic Technologies for Computing (CO-OP) conducted by George Mason University and the Honeywell Technology Center in 1996.

References

1. J. M. Sasian and D. A. Baillie, "Simple technique for out-of-focus feature alignment," *Opt. Eng.* **34**, 564-566 (1995).
2. S. K. Patra, J. Ma, V. H. Ozguz, and S. H. Lee, "Alignment issues in packaging for free-space optical interconnects," *Opt. Eng.* **33**, 1561-1570 (1994).
3. B. Robertson, Y. Liu, G. C. Boisset, M. R. Taghizadeh, and D. V.

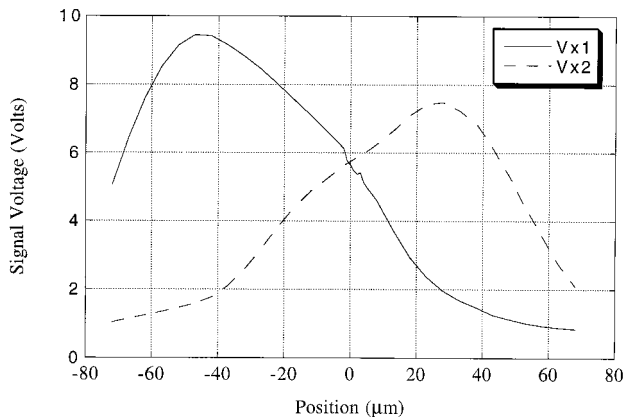


Fig. 11. Experimental measurement of the signal voltages V_{x1} and V_{x2} versus the translation error.

- Plant, "In situ interferometric alignment systems for the assembly of microchannel relay systems," *Appl. Opt.* (to be published).
4. J. Jahns and S. J. Walker, "Imaging with planar optical systems," *Opt. Commun.* **76**, 313–317 (1990).
 5. J. Jahns, Y. H. Lee, C. A. Burrus, Jr., and J. L. Jewell, "Optical interconnects using top-surface-emitting microlasers and planar optics," *Appl. Opt.* **31**, 592–597 (1992).
 6. D. V. Plant, B. Robertson, H. S. Hinton, M. H. Ayliffe, G. C. Boisset, D. J. Goodwill, D. Kabal, R. Iyer, Y. S. Liu, D. R. Rolston, M. Venditti, T. H. Szymanski, W. W. Robertson, and M. R. Taghizadeh, "Optical, optomechanical, and optoelectronic design and operational testing of a multistage optical backplane demonstration system," in *Proceedings of the Conference on Massively Parallel Processing Using Optical Interconnections (MPPOI)* (IEEE Computer Society, Los Alamitos, Calif., 1996), pp. 306–312.
 7. T. H. Szymanski and H. S. Hinton, "Reconfigurable intelligent optical backplane for parallel computing and communications," *Appl. Opt.* **35**, 1253–1268 (1996).
 8. T. H. Szymanski and H. S. Hinton, "Architecture of a terabit free-space intelligent optical backplane," *J. Parallel Distrib. Comput.* (to be published).
 9. F. B. McCormick, F. A. P. Tooley, T. J. Cloonan, J. M. Sasian, H. S. Hinton, K. O. Mersereau, and A. Y. Feldblum, "Optical interconnections using microlens arrays," *Opt. Quantum Electron.* **24**, 265–277 (1992).